Spontaneous symmetry breaking and electronic and dielectric properties in commensurate La_{7/4}Sr_{1/4}CuO_{4} and La_{5/3}Sr_{1/3}NiO_{4}

J. Petersen, F. Bechstedt, J. Furthmüller, and L. M. Scolfaro

Phys. Rev. B **97**, 195129 — Published 15 May 2018

DOI: 10.1103/PhysRevB.97.195129

Spontaneous symmetry breaking, electronic, and dielectric properties in commensurate LSCO and LSNO

J. Petersen,[1] F. Bechstedt,[2] J. Furthmüller,[2] and L. M. Scolfaro[1*]

[1]Department of Physics, Texas State University, 78666 San Marcos, Texas, USA

[2]Institut für Festkörpertheorie und -optik, Friedrich-Schiller-Universität Jena, Max-Wien-Platz 1, D-07743 Jena, Germany

Abstract

Complex ordered phases involving spin and charge degrees of freedom in condensed matter, such as layered cuprates and nickelates, are exciting but not well-understood solid-state phenomena. The rich underlying physics of the overdoped high-temperature superconductor $La_{7/4}Sr_{1/4}CuO_4$ and colossal dielectric constant insulator $La_{5/3}Sr_{1/3}NiO_4$ is studied from first principles within Density Functional (Perturbation) Theory, including an effective Hubbard potential U for the exchange and correlation of d orbitals. Charge density wave (CDW) and spin density wave (SDW) order is found in both materials, where the stripes are commensurate with the lattice. The SDWs are accompanied by complex antiferromagnetic spin arrangements along the stripes. The first series of conduction bands related to the pseudogap observed in the cuprate are found to be directly related to CDW order, while the colossal dielectric constant in the nickelate is demonstrated to be a result of vibronic coupling with CDW order. Differences between the two oxides are related to how the stripes fill with carriers.

*Contact Author: lscolfaro@txstate.edu

I. INTRODUCTION

Since the discovery of high-temperature superconductivity (HTSC) in a doped antiferromagnetic (AF) cuprate in 1986 [1], the scientific community has uncovered a host of ordered phenomena in related materials. Such ordering includes, but certainly is not limited to, charge-density waves (CDWs) and spin-density waves (SDWs). A CDW is self-organized charge density, generally from hole-doping or oxygen interstitials, arranged in periodic patterns at the atomic scale, below a charge-ordering temperature T_{CO}. Local magnetic moments are reduced at sites where the excess charge density is greatest, which act as domain walls to AF order, and a SDW manifests as the resulting periodic yet incommensurate magnetic order, of lattice period twice that of the CDW, occurring below a spin-ordering temperature T_{SO}, where generally $T_{SO} < T_{CO}$. A combination of CDW and SDW aligns in "stripes" in the two-dimensional Cu-O or Ni-O bonding planes, which are separated by Mott insulating layers. Stripe physics is an active area of research, both experimentally and theoretically, since the relation between stripes and the formation, coupling, and filling to HTSC, as well as the influence of competing orders due to charge, spin, orbital, and lattice fluctuations are heavily debated [2].

Hückner et al. found convincing experimental evidence that the enhanced commensurability of stripes at x = 1/8, in $La_{2-x}Ba_xCuO_4$, resulted in suppression of HTSC [3]. They showed that the same composition can exhibit slight superconducting (SC) behavior in the Cu-O planes [4,5]. For Sr concentration slightly less than 1/8, replacing Ba by Sr, in electrochemically oxygen-doped $La_{2-x}Sr_xCuO_{4+\delta}$, excess oxygen congregates as interstitials, such that hole concentration in the bulk equals 1/8 [6]. This concentration is known as the 1/8 anomaly [7]. Nearly isostructural yet insulating $La_{2-x}Sr_xNiO_4$ (LSNO) is well known to exhibit stripes and have a colossal dielectric constant (CDC) into the GHz range, with its highest values reported being ~10^6–10^7 for a Sr concentration of x = 1/8, where

the colossal value is interpreted as resulting from spatial modulation of hole charge [8,9]. However, diffraction measurements on LSNO have shown that neither the charge ordering transition nor the magnetic ordering transition is well defined [10,11].

In addition to being of interest for oxide electronics, comparing stripe physics of LSNO with $La_{2-x}Sr_xCuO_4$ (LSCO) can help illuminate the mechanism(s) behind HTSC in the cuprates, due to different carrier filling. Recently, Coslovich et al. detected a mid-infrared optical gap in LSNO, with x = ¼. They interpreted it as having pseudogap (PG) characteristics, which they attributed to electronic localization (disorder), rather than stripes (order) [12]. In the cuprates, two d orbital gaps of Cu $x^2 - y^2$ (i.e. d orbital) character are present – the PG and the SC gap. The SC gap is the lower energy gap where Cooper pair formation occurs in the Cu-O plane below a critical temperature T_C, while the PG is at higher energy and is present below a temperature T*, where $T^* > T_C$. Both gaps exhibit a Fermi surface along the nodal bonding direction in the Cu-O plane and have Cu $x^2–y^2$ and O p character. The origin of the PG in the cuprates is heavily debated [7,13], and is one of the most prominent unsolved problems in condensed matter physics, along with the mechanism(s) behind HTSC, and whether a connection between the two is significant. In this work, charge and spin ordering, electronic structure, and dielectric response are theoretically characterized for highly commensurate x=1/3 LSNO and x=1/4 LSCO from first principles.

Experimentally, below x = 1/2, the nickelate remains insulating [14,15], while the cuprate is past the SC limit at x = 0.3 and is semi-metallic [16]. The concentration of x = 1/3 has been found to show the most commensurate stripe ordering for x < 1/2 in LSNO [15,17]. At these critical Sr doping concentrations, well-defined fillings of the stripe atoms in the Ni-O and Cu-O planes may occur. The two nearly isostructural layered materials crystallize in the tetragonal crystal system with I4/mmm space group without doping (doped supercells shown in Figures 1 and 2). They are model materials to study the interplay of charge, spin, and lattice degrees of freedom. In particular, the d-electron shells of

the transition metal atoms Ni and Cu, which differ by only one electron, allow investigations of the influence of band filling. Electronic structure of the resulting stripe phases is analyzed by band structure and projected density of states (PDOS). The frequency-dependent dielectric tensor allows conclusions about interband transitions and the static dielectric constants of LSNO. The vibronic contribution to the static dielectric constants is calculated via Density Functional Perturbation Theory, where it is found that significant vibronic-CDW coupling accounts for the huge values of the CDC.

The dielectric functions of LSCO are not calculated, because of its semi-metallic nature, which requires the inclusion of Drude-like terms to account for intraband transitions, yet the electronic structure of x = ¼ LSCO is compared to calculations of x = 1/3 LSNO. The concentration of x = ¼ in LSCO lies within the overdoped regime of the SC dome. Božović and colleagues found recently that the strongly interacting electronic system in overdoped cuprates differs fundamentally from that which is expected from the Bardeen–Cooper–Schrieffer (BCS) theory of superconductivity [18, 19]. The dopant concentration of x = ¼ is integrally commensurate with the lattice, making it particularly suitable for study within a many-body theory. Here, two sets of gaps are found in the electronic structure of overdoped LSCO which have orbital character bearing striking resemblance to the PG and SC gap.

II. THEORETICAL METHODS

Theoretical studies of HTSC materials generally use the Hubbard model or the t-j model in two dimensions. Stripe physics can be predicted via these methods, as well, as shown by Chen [17] or Zaanen and Littlewood [20]. However, a different approach is necessary to go beyond model Hamiltonians and perform self-consistent, almost parameter-free studies in three dimensions. Here, we theoretically characterize the impurity-induced excited states of x = 1/4 LSCO, using first principles, by comparing directly with optical calculations of insulating x = 1/3 LSNO, within the independent

particle approximation (IPA) [21]. Ground state calculations were performed within Density Functional Theory (DFT), including spin polarization, using the Vienna ab initio Simulation Package (VASP). The Projector-Augmented Wave method [22] was used to generate pseudopotentials, where the 4s, and the 3p and 3d electrons of Ni and Cu are treated as valence electrons, but all-electron wave functions are simulated effectively. Because of their strong localization, the d electron systems are highly-correlated, so exchange and correlation are treated with an improvement beyond the Local Spin Density Approximation (LSDA) in this work. To account for correlation of d electrons, the effective Hubbard U – J interaction of Dudarev, et al. (LSDA + U) [23] is included. The effective Hubbard U – J value was varied until magnetic properties were reproduced for x = 0, i.e., zero Sr doping. The plane wave cutoff energy was chosen to be 520 eV. Due to the large lattice constants, only the gamma point is necessary in order to calculate total energy accurately. To ensure this assumption, the k points were increased to Γ-centered meshes of 2 × 2 × 2 for LSNO and 2 × 2 × 1 for LSCO, taking care to include the high-symmetry points of main interest – Γ, M, X, and Y – and total ground-state energy agreed with the cases of fewer k points (-55.722 and -54.665 eV/chemical formula unit for LSNO and LSCO, respectively). The number of sampling points to calculate density of states (DOS) was systematically increased until a small Gaussian smearing parameter of 0.03 eV was used in the case of LSNO, with 0.01 eV for the optical calculations, within the IPA. A Methfessel-Paxton smearing parameter of 0.1 eV was used in the case of LSCO to account for the details of the Fermi surface. Collinear spins were applied within the LSDA + U approach. However, the band degeneracies and spin orientations were checked with unrelaxed noncollinear calculations.

III. RESULTS AND DISCUSSION

A. Structure, charge and spin densities

The Dudarev method has been shown to describe the electronic structure accurately in the materials studied here [24, 25]. However, it has been shown rigorously that choice of U value in highly-correlated MnTe can affect physical properties, such as phase stability, while other properties are described more accurately with different values [26]. Furthermore, the works of Blaha et al. [25] and Rivero et al. [27] clearly show that choice of U value in related layered cuprates affects electronic structure and local magnetization significantly, and an appropriate value is necessary to describe the ground state accurately. Since large U values are prone to getting trapped in local energetic minima [28], here, U – J values were varied from 0 to 8 eV in the test cases of x = 0, i.e. La_2NiO_4 and La_2CuO_4, to optimize the effective Hubbard parameter U – J. For comparison with the x = 0 cases, experimentally determined magnitude of Ni site magnetization in antiferromagnetic La_2NiO_4 is 1.68 μ_B [29], while it is 0.4 μ_B on Cu sites in La_2CuO_4 [30]. Local magnetization and magnetic coupling constants were calculated in both systems, for x = 0, over a range of Hubbard U values, within the Dudarev approximation of an effective U – J [23]. The chosen effective U – J values used in this work of 6.62 and 5.0 eV, for LSNO and LSCO, respectively, correspond to magnetic coupling constants of 33 and 117 meV, while experimental values are 30 [31] and 128-135 meV [32, 33]. Magnetic coupling constants were calculated according to the method outlined by Feng et al [34]. For LSNO, due to the more dramatic reduced magnetic moment on stripe-centered Ni sites, the U – J value was reduced by 0.5 eV on metal cation sites where CDW was found to be densest, as suggested by Yamamoto et al. [35] and in agreement with arguments of Anisimov et al [36]. Using these U – J values, lattice parameters were optimized for the x = 0 cases via the Murnaghan equation of state (results for Murnaghan fits of LSNO over the range of U – J values shown in Figure S1 (a) [51]). In the doped

systems, La was directly substituted by Sr, and full ionic relaxation resulted in forces less than 3 meV/Å on each ion. For the x = 0 cuprate, contrary to results of Pesant, et al. [37], the magnetic coupling constant was found to increase with U – J up to 5.0 eV, where it plateaus around 117 meV. Magnetic properties were the focus when finding an optimal effective U – J, since the SDW formation in the doped systems is critically important.

The results of the test cases on the intrinsic materials are summarized in Figure S1 for La_2NiO_4 and Figure S2 for La_2CuO_4 [51]. In Figure S1 (b), magnetic coupling constant is shown as a function of U – J, and an intersection with the experimental value (red dashed line) can be seen at two points. In Figure S1 (c), the energy band gap approaches the experimental value (red dashed line) as U – J is increased. Of the two intersection points in Figure S1(b), only one has a finite energy band gap. The U – J value used by Yamamoto et al. [35] (6.62 eV) was found here to yield a magnetic coupling constant close to experiment within the range of an open band gap. Therefore, this value was used in the doped system for non-stripe-centered Ni. For stripe-centered Ni, as mentioned above, where CDW is densest, U – J is reduced by 0.5 eV to 6.12 eV. Similar calculations were performed on La_2CuO_4, and Figure S2 shows the data of the magnetic coupling constant over a range of U – J values. Here, the magnetic coupling constant plateaus, so the U – J value chosen for the doped system LSCO corresponds to the onset of the plateau (5 eV). For a summary of U – J values used, see Table S1 [51].

The tetragonal undoped primitive cells were translated to orthorhombic supercells, with CDW and SDW commensurability in mind. The 1% orthorhombic distortion of the I4/mmm tetragonal primitive cell in LSCO is neglected. However, tilt of NiO_6 and CuO_6 octahedra is taken into account in both structures and is found to affect magnetic order substantially in the cuprate. The supercell size was increased to $3\sqrt{2} \times \sqrt{2} \times 1$ for x = 1/3 LSNO and $8 \times 2 \times 1$ for x = 1/4 LSCO and found to be sufficient to describe charge and spin ordering for the Sr concentrations considered (Figures 1 and 2). Ni-O-Ni distance was found to be 3.81 Å, and Cu-O-Cu distance is 3.76 Å along the bonding direction. In

LSNO, each Ni-O plane has two stripe-centered Ni and four non-stripe-centered Ni, while in LSCO, four Cu are stripe-centered, and eight are non-stripe-centered. The vertical size of the supercells in Figures 1 and 2 may lead to a minimal interplanar correlation. Indeed, Zimmerman, et al. showed experimentally that stripes are rotated 90 degrees in adjacent planes in $La_{1.48}Nd_{0.4}Sr_{0.12}CuO_4$ [38]. To consider the rotation here, a larger unit cell for LSNO should have dimensions $3\sqrt{2} \times 3\sqrt{2} \times s$, where the integer $s > 1$ would allow simulation of staggering, or periodic shifting, of stripes every other layer [3]. The $\sqrt{2}$ is introduced to describe CDW periodicity, since stripes in LSNO are oriented at 45 degrees to Ni-O bonds in the Ni-O planes. CDW periodicity is then $3\sqrt{2}/2$, while it is $3\sqrt{2}$ for SDW. In comparison, the lateral unit cell of the cuprate is quite different, since the stripes align along Cu-O bonds [3]. The unit cell approximation here is necessary, due to the sheer number of atoms in the calculation – 84 for the case of LSNO and 224 for LSCO.

To maintain commensurability, the size of the cell depends critically on Sr concentration, since the sites at which La is substituted by Sr are found to affect CDW and SDW ordering drastically. This agrees with the results of Lloyd, et al., which indicate pinning of CDW to impurity location [39]. Thus, care was taken in choosing the initial magnetization on each Ni or Cu site and the position of the Sr atoms in each cell before minimizing the total energy in the ground state. Only certain configurations of Sr dopants were found to produce CDW and SDW in the Cu-O or Ni-O planes. The hole density congregates on the Cu or Ni nearest to the Sr, depending on spin, indicating that CDW and SDW are intimately related and dependent upon Sr position. The Sr positions are ordered with the same lattice periodicity as the CDW, in both oxides. The original lattice symmetry is spontaneously broken. There have been several cases of experimentally observed oxygen interstitial lattice ordering in $La_2NiO_{4.125}$ [40-43]. Moreover, Lee, et al. observed interstitial oxygen order every fourth La_2O_2 layer in the HTSC $La_2CuO_{4.11}$ [44]. Contrary to the case of oxygen interstitials, several experimental reports show Sr dopants are disordered in LSNO, which prevents long-range stripe order [17,43,45,46]. With CDW

localization being dependent upon dopant position in the lattice, Sr disorder will result in a smectic phase at temperatures approaching 0 K, and may be nematic at finite temperatures, as found recently in experiment [47].

In order to illustrate both density wave formations in Figures 1 and 2, the formation of stripes in the Ni-O and Cu-O planes are shown in Figures 3 and 4, in planes perpendicular to the c axis. The magnetic unit cells, which are twice the lateral periodicity of the CDW, are commensurate with the SDW. The Ni-O or Cu-O planes are separated by insulating LaO_2 layers, which are doped periodically with Sr. Each Sr provides one hole to one Ni or Cu in the nearest plane. The charge and spin distributions in Figures 3 and 4 are repeated along the vertical axis in a Bloch-like fashion (3x for LSNO and 4x for LSCO) to better illustrate the resulting density waves. Peaks correspond to holes donated by nearest-neighbor Sr which is out of the plane. Sites of reduced magnetic moment have a gray circle in LSCO and gray arrow in LSNO, and in both cases, these sites coincide with greatest charge density in the excited state considered. Since the Ni atoms form square lattices bridged by O neighbors, with a distance of a = 3.81 Å, stripes of hole charge are aligned at 45 degrees to the Ni-O bonding direction in LSNO, giving rise to CDWs separated by two Ni of opposite spin. This finding is in complete agreement with neutron scattering data [48]. In contrast to LSNO (Figure 3), in LSCO, charge stripes and reduced magnetic moment sites form zig-zag chains, as shown in Figure 4.

At Ni sites nearest to Sr, where the CDW has the greatest density in LSNO, the magnetic moment is reduced by ~0.7 μ_B, while moments of Cu sites at CDW nodes are reduced almost completely in LSCO. A complex spin pattern is visible far away from the linear antiferromagnetic ordering along the stripes for LSNO. In each case, CDW nodes are found to be centered on one Ni or Cu ion with additional localization on neighboring O ions in the 2D plane (Figure 1), indicating coupling between Sr position, CDW, and SDW. In LSNO (LSCO), Sr and CDW periodicities are both $3\sqrt{2}a / 2$ (4a), while SDW periodicity is $3\sqrt{2}a$ (8a). Our results suggest that these large primitive cell

sizes should be considered when determining wave vectors in experimental characterization of similar materials exhibiting stripes. The hole charge density plots in Figures 3 and 4 were found from the square of the modulus of the wavefunction of the first excited states in LSNO and LSCO. Incidentally, both sets of impurity conduction bands in LSCO give rise to CDW with nodes located among Cu nearest to Sr impurity. The SDW corresponds to magnetic moments on Ni sites normal to Ni-O bonding plane of -1.62, 1.62, 0.92, -1.63, 1.63, -0.92 μ_B, where reduced moment Ni sites with stripe localization have local magnetic moments of 0.92 μ_B. For x = 1/4 LSCO, magnetic moments on Cu sites normal to the Cu-O plane are found to be 0.08, 0.41, -0.46, 0.47, -0.08, -0.41, 0.46, -0.47 μ_B, where reduced moment Cu sites with stripe localization have local magnetic moments approaching zero μ_B. In both oxides, commensurability is satisfied, and the total magnetization of the unit cell is zero, which agrees with the Dynamical mean-field theory (DMFT) calculations of Weber and colleagues [49]. Both the Cu z^2 / O p_z hybridization and local magnetic moments are described effectively in the doped systems with the chosen U – J parameter.

Which La sites are substituted by Sr affects results significantly, especially the commensurability of CDW and SDW. The concentrations x = 1/3 (LSNO) and x = ¼ (LSCO) lead to high commensurability between the density waves and the underlying atomic lattice, for periodic Sr. Alternative Sr concentrations and positions in the lattice modify charge density and spin orientation, resulting in incommensurate CDWs and SDWs in the chosen unit cells, along with a net magnetization which is to be avoided. Figures 3 and 4 show the commensurability of CDWs and SDWs with their respective lattices. Hole density of the first excited states in the (001) plane of x = 1/3 LSNO and x = 1/4 LSCO is presented, respectively, at z = 1/2, using collinear spin, where interplanar correlation is found to be negligible. In this limit, spin collinearity is an excellent approximation which is used throughout the rest of the study; however, it should be noted that a test calculation (unrelaxed) with noncollinear spins gave rise to more pronounced interlayer coupling. Spin-dependent hole charge

density of the spin up and spin down degenerate bands have similar magnitudes at each stripe location in the plane.

B. Electronic and optical properties

Whether the excited states of the PG or SC gap are attributed to charge stripe can be determined by segregating PDOS of stripe-centered metal ions from those of non-stripe-centered ones, as demonstrated by Yamamoto, et al. on x = 1/3 and x = ¼ LSNO [35]. Both the PG and SC gap in x = 1/4 LSCO are characterized as being transitions to Cu sites at which CDWs are localized, along with O p. Cu sites without hole localization, where magnitude of magnetic moments are strongest, analogous to x = 0, exhibit a normal gap, which is found at a different transition energy than the PG or SC gap. The first excited state found in LSNO within the Born-Oppenheimer approximation, while of x^2-y^2 orbital character, does not resemble the PG found experimentally by Coslovich and colleagues [12]. Electronic structure was calculated for the obtained CDW and SDW ground states of x = 1/3 LSNO. In Figure 5, the band structure and PDOS of LSNO clearly show an insulating ground state. A fundamental direct gap of 1 eV is found at the Y point of the Brillouin zone (BZ). In Figure 5(a), the degeneracy of hole bands is lifted, with respect to the plane in which the hole is localized, however degeneracy remains throughout most of the BZ. The four bands of the conduction band minimum (CBM) are degenerate throughout most of the BZ, but degeneracy is lifted along the high symmetry lines M to Y and Γ to Y. The four bands correspond to two different nodes of the CDW in each of the two Ni-O planes in the unrelaxed noncollinear test calculation. It is the planar degeneracy that is lifted – not that of spin. To characterize the bands, figures 5(b), 5(c), and 5(d) correspond to PDOS calculations projected onto non-stripe-centered Ni, stripe-centered Ni, and O, respectively. Our results show $x^2 - y^2$ orbital character of the CBM, along with some presence of O p. Some presence of the z^2 orbital can be seen at the valence band maximum (VBM), as well. Our results widely agree with those of Yamamoto, et al.

[35], however, we observe a much larger band gap along with more states above the Fermi energy. Technically speaking, this is due to the points used to calculate the PDOS, along with a small broadening parameter used for Gaussian smearing. Furthermore, an unrelaxed collinear test calculation resulted in a band gap of 0.2 eV. Thus, the relaxation is found to increase the band gap significantly. In the electronic structure, a CBM state exists for each change in energy related to high symmetry points in the BZ. These states are mostly localized to the stripe-centered Ni sites, along with some contributions from neighboring O (Figure 5a(c)). Each of these two states gives rise to an optical transition for in-plane light polarization, resulting in a peak in Figure 5(e). Although the LSDA + U approach cannot provide accurate conduction band eigenvalues relative to the VBM, the character and symmetry of the bands are well described, so one can make qualitative spectral rather than quantitative energetic conclusions.

The imaginary parts of the frequency-dependent dielectric function characterize the optical absorption parallel to the Ni-O plane (ε_{xx}) and parallel to the c-axis (ε_{zz}). Two transitions, one at Y, for light polarized parallel to stripe direction in the Ni-O plane, from O p_y to Ni $x^2 - y^2$, and a higher transition at X, perpendicular to stripe direction yet in the Ni-O plane, from O p_x to Ni $x^2 - y^2$. Both fulfill the angular momentum selection rule and indicate a charge-transfer gap. Transitions are forbidden for polarization along the c-axis at low energy. Only those at the zone boundary are visible.

While no PG character is found in LSNO, it should be noted that the electronic structure calculations of Figure 5 were performed within the Born-Oppenheimer approximation. Coslovich, et al. measured a PG at finite temperatures in x = ¼ LSNO, with a decrease in optical conductivity with temperature at low energy [12]. As they suggest, the PG may be attributed to contributions of the vibrating lattice in the stripe-ordered geometry. The results of Homes, et al. confirm that low energy mid-gap states are not present at low temperature [40]. Lloyd-Hughes et al. found negligible optical conductivity at low temperature for x = 1/3 yet a substantial increase for incommensurate x = 0.275

[39]. Our calculations suggest that the optical conductivity (imaginary part of the dielectric function multiplied by the frequency) of the PG reduces to zero at zero temperature for commensurate samples, yet transitions are apparent at low energy.

The real parts of the calculated dielectric functions describe light refraction and propagation. Their $\omega \rightarrow 0$ limits determine the electronic contribution to the dielectric properties of LSNO. The dielectric results are summarized in Table 1. We find static electronic dielectric constants $\epsilon_{ii}^{\infty} = \epsilon_{ii}(0)$ of the order of magnitude known for semiconductors with similar fundamental gaps. Thereby, the components parallel to the layers are somewhat larger than the component in the c direction. Local field effects increase (decrease) the dielectric constants perpendicular (parallel) to the c axis slightly. Adding the static polarizabilities α_{ij} of the vibrating lattice, the tensor of the static dielectric constants $\epsilon_{ij}^{0} = \epsilon_{ij}^{\infty} + \alpha_{ij}$ appear. The anisotropic phonon contributions to the dielectric properties of x = 1/3 LSNO with stripe ordering are investigated in the DFPT framework [50]. The lattice polarizabilities in Table 1, the phonon or vibronic contributions, are much larger than the static electronic polarization contributions. Moreover, they show a large effect due to the stripe anisotropy. In particular, total in-plane values of the order of 50 are predicted by the ab initio calculations. The dielectric tensor is diagonal in agreement with the structural finding of the primitive orthorhombic character of the LSNO system. Our results compare qualitatively well with the low temperature measurements of Filippi, et al [14]. They attribute the value of about 100 to charge ordering in the Ni-O plane, whereas the results presented here indicate that it is the vibronic interaction with the CDW in the Ni-O plane that is the dominant mechanism behind the CDC in LSNO. It has been reported previously that phonon coupling to CDW and SDW is much more pronounced in LSNO than in the cuprates [20], so vibronic contributions to physical properties of LSCO are not investigated here.

A direct comparison between the electronic properties of x = 1/3 LSNO and x = 1/3 LSCO is not very helpful, since x = 1/3 LSCO is overdoped and slightly metallic (not superconducting). The

system considered here is x = ¼ LSCO, which is between the optimal doping concentration of x = 0.17 and the SC limit of x = 0.3 [16]. The metallic character can be seen clearly in the band structure (Figure 6a) along Γ – M, i.e., the nodal direction, from (0, 0) to (π, π). The Fermi energy crosses the uppermost two valence bands, leading to hole pockets near the zone boundaries. Two series of conduction bands not present in the undoped case appear in the band structure between 0.2 and 0.7 eV. The lower one has orbital character related to the SC gap, whereas the one above that is the excited state of the PG. The conduction states above the two gaps of the doped system form the normal gap, correspondent to the intrinsic x = 0 gap. The PDOS in Figure 6d shows that along with the SC gap, PG, and normal gap all have a strong O 2p character. The Cu $x^2 - y^2$ and O p bond leads to optical transitions to the SC gap and the PG along Γ – X with the same character, as found in the case of LSNO. The Cu z^2 / O p_z hybridization can be seen at the Fermi surface. The $x^2 - y^2$ state ascribed to non-stripe-centered Cu forms the normal gap (Figure 6b), while the excited states of the SC gap and PG of $x^2 - y^2$ character are directly related to the stripe-centered Cu sites (Figure 6c). Our results clearly prove the proposal of Tranquada, et al., that only states aligned with the stripes are gapped [5]. This fact confirms that the PG is directly caused by CDW, i.e., the symmetry break.

IV. CONCLUSIONS

By means of first-principles calculations, we have shown the ground states of x = 1/3 LSNO and x = ¼ LSCO, including SDW order. The impurity-related conduction bands are investigated here by studying electronic structure of commensurate x = ¼ LSCO, where they are found to be directly related to CDW. Additionally, in the case of x = 1/3 LSNO, the gap character is studied by means of the optical absorption. Electronic structure agrees with experimental results for both systems considered. We demonstrated that CDW and SDW orders are inherently dependent on Sr position in the lattice. Nematic or smectic behavior should be observed experimentally in the case of disordered Sr dopants.

We have shown that the pseudogap originates from the Cu $x^2 - y^2$ states located around stripe-centered Cu sites, along with O p. The Cu z^2 / O p_z hybridization at the Fermi surface is correctly described by the LSDA + U method. The CDC of LSNO was studied by investigating both the electronic and vibronic contributions to the dielectric properties. The lattice polarizability and vibronic interaction with the CDW in the NiO plane is found to be the main contribution to the colossal value. In addition to the reasonable static electronic contributions, the lattice polarizabilities become most important, in particular for the component of the dielectric tensor perpendicular to the c axis.

ACKNOWLEDGMENTS

The authors would like to thank Susumu Yamamoto for the helpful discussion. Also, JP and LMS would like to acknowledge Texas State University for financial support under DOD grant HBCU/MI W911NF-15-1-0394.

[1] J. G. Bednorz, & K. A. Müller, Possible high Tc superconductivity in the Ba-La-Cu-O system. Zeitschrift für Phys. B Condens. Matter **64,** 189–193 (1986).

[2] P. A. Lee, N. Nagaosa, & X. G. Wen, Doping a Mott insulator: Physics of high-temperature superconductivity. Rev. Mod. Phys. **78,** (2006).

[3] M. Hücker, M. v. Zimmermann, G. D. Gu, Z. J. Xu, J. S. Wen, Guangyong Xu, H. J. Kang, A. Zheludev, and J. M. Tranquada. Stripe order in superconducting $La_{2-x}Ba_xCuO_4$ ($0.095 \leq x \leq 0.155$). Phys. Rev. B 83, 104506 (2011).

[4] Q. Li, M. Hücker, G. D. Gu, A. M. Tsvelik, & J. M. Tranquada, Two-dimensional superconducting fluctuations in stripe-ordered $La_{1.875}Ba_{0.125}CuO_4$. Phys. Rev. Lett. **99,** 4–7 (2007).

[5] J. M. Tranquada, G. D. Gu, M. Hücker, Q. Jie, H.-J. Kang, R. Klingeler, Q. Li, N. Tristan, J. S. Wen, G. Y. Xu, Z. J. Xu, J. Zhou, and M. V. Zimmermann**.** Evidence for unusual superconducting correlations coexisting with stripe order in $La_{1.875}Ba_{0.125}CuO_4$. Phys. Rev. B 78, 1–13 (2008).

[6] H. E. Mohottala, Barrett O. Wells, Joseph I. Budnick, William A. Hines, Christof Niedermayer, Linda Udby, Christian Bernhard, Arnold R. Moodenbaugh, and Fang-Cheng Chou. Phase separation in superoxygenated $La_{2-x}Sr_xCuO_{4+y}$. Nat. Mater. **5,** 377–382 (2006).

[7] E. Fradkin, S. A. Kivelson, & J. M. Tranquada, Colloquium: Theory of intertwined orders in high temperature superconductors. Rev. Mod. Phys. **87,** 457–482 (2015).

[8] S. Krohns, P. Lunkenheimer, Ch. Kant, A. V. Pronin, H. B. Brom, A. A. Nugroho[4], M. Diantoro, and A. Loidl. Colossal dielectric constant up to gigahertz at room temperature. Appl. Phys. Lett. **94,** 1–4 (2009).

[9] A. Podpirka, A., Tselev, A. & Ramanathan, S. Synthesis and frequency-dependent dielectric properties of epitaxial $La_{1.875}Sr_{0.125}NiO_4$ thin films. J. Phys. D. Appl. Phys. **45,** 305302 (2012).

[10] C. Hess, B. Buchner, M. Hücker, R. Gross, & S. W. Cheong, Phonon thermal conductivity and stripe correlations in $La_{2-x}Sr_xNiO_4$ and $Sr_{1.5}La_{0.5}MnO_4$. Phys. Rev. B **59,** 10397–10400 (1999).

[11] C.-H. Du, M. E. Ghazi, Y. Su, I. Pape, P. D. Hatton, S.D. Brown, W. G. Stirling, M. J. Cooper, S. –W. Cheong. Critical Fluctuations and Quenched Disordered Two-Dimensional Charge Stripes in $La_{5/3}Sr_{1/3}NiO_4$. Phys. Rev. Lett. **84,** 3911–3914 (2000).

[12] G. Coslovich, B. Huber, W. -S. Lee, Y. -D. Chuang, Y. Zhu, T. Sasagawa, Z. Hussain, H. A. Bechtel, M. C. Martin, Z. -X. Shen, R. W. Schoenlein, R. A. Kaindl. Ultrafast charge localization in a stripe-phase nickelate. Nat. Commun. **4,** 2643 (2013).

[13] S. Huefner, M. A. Hossain, A. Damascelli, & G. A. Sawatzky, Two Gaps Make a High-Temperature Superconductor? Reports Prog. Phys. **71,** 62501 (2008).

[14] M. Filippi, B. Kundys, S. Agrestini, W. Prellier, H. Oyanagi, H, N. L. Saini. Charge order, dielectric response, and local structure of $La_{5/3}Sr_{1/3}NiO_4$ system. J. Appl. Phys. **106,** 104116 (2009).

[15] H. Yoshizawa, T. Kakeshita, R. Kajimoto, T. Tanabe, T. Katsufuji, and Y. Tokura. Stripe order at low temperatures in $La_{2-x}Sr_xNiO_4$ for $1/3 < x < 1/2$. Phys. Rev. B 61, R854 (2000).

[16] R. A. Cooper, Y. Wang, B. Vignolle, O. J. Lipscombe, S. M. Hayden, Y. Tanabe, T. Adachi, Y. Koike, M. Nohara, H. Takagi, C. Proust, N. E. Hussey. Anomalous criticality in the electrical resistivity of $La_{2-x}Sr_xCuO_4$. Science **323,** 603–607 (2009).

[17] C. Chen, S. Cheong, & A. Cooper, Charge modulations in $La_{2-x}Sr_xNiO_{4+y}$: Ordering of polarons. Phys. Rev. Lett. **71,** 2461–2464 (1993).

[18] I. Božović, X. He, J. Wu, & A. T. Bollinger, Dependence of the critical temperature in overdoped copper oxides on superfluid density. Nature **536,** 309–311 (2016).

[19] J. Zaanen, Superconducting electrons go missing. Nature **536,** 282–283 (2016).

[20] J. Zaanen, & P. B. Littlewood, Freezing electronic correlations by polaronic instabilities in doped La_2NiO_4. Phys. Rev. B **50,** 7222–7225 (1994).

[21] M. Gajdoš, K. Hummer, G. Kresse, J. Furthmüller, & F. Bechstedt, Linear optical properties in the projector-augmented wave methodology. Phys. Rev. B **73,** 45112 (2006).

[22] P. Blöchl, Projector augmented-wave method. Phys. Rev. B **50,** 17953 (1994).

[23] S. L. Dudarev, S. Y. Savrasov, C. J. Humphreys, & A. P. Sutton, Electron-energy-loss spectra and the structural stability of nickel oxide: an LSDA+U study. Phys. Rev. B **57,** 1505–1509 (1998).

[24] M. T. Czyyk, & G. A. Sawatzky, Local-density functional and on-site correlations: The electronic structure of La_2CuO_4 and $LaCuO_3$. Phys. Rev. B **49,** 14211–14228 (1994).

[25] P. Blaha, K. Schwarz, & P. Novák, Electric field gradients in cuprates: Does LDA+U give the correct charge distribution? Int. J. Quantum Chem. **101,** 550–556 (2005).

[26] M. Krause, & F. Bechstedt, Structural and magnetic properties of MnTe Phases from Ab initio calculations. J. Supercond. Nov. Magn. **26,** 1963–1972 (2013).

[27] P. Rivero, I. de P.R. Moreira, & F. Illas, Electronic structure of single-layered undoped cuprates from hybrid density functional theory. Phys. Rev. B **81,** 1–12 (2010).

[28] B. Meredig, A. Thompson, H. A. Hansen, C. Wolverton, & A. Van De Walle, Method for locating low-energy solutions within DFT+U. Phys. Rev. B **82,** 2–6 (2010).

[29] J. Rodriguez-Carvajal, M. T. Fernandez-Diaz, & J. L. Martinez, Neutron diffraction study on structural and magnetic properties of La_2NiO_4. J. Phys. Condens. Matter **3,** 3215–3234 (1991).

[30] D. Vaknin, S. K. Sinha, D. E. Moncton, D. C. Johnston, J. M. Newsam, C. R. Safinya, and H. E.

King, Jr. Antiferromagnetism in La_2CuO_{4-y}. Phys. Rev. Lett. 58, 2802–2805 (1987).

[31] S. Itoh, Kazuyoshi Yamada[2], Masatoshi Arai, Yasuo Endoh, Yoshikazu Hidaka, and Syoichi Hosoya. Spin Dynamics on Two-Dimensional Heisenberg Antiferromagnets –High Energy Neutron Inelastic Scattering from La_2CuO_4 and La_2NiO_4. J. Phys. Soc. Japan **63,** 4542–4549 (1994).

[32] P. E. Sulewski, P. A. Fleury, K. B. Lyons, S. W. Cheong, & Z. Fisk, Light scattering from quantum spin fluctuations in R_2CuO_4 (R=La, Nd, Sm). Phys. Rev. B **41,** 225–230 (1990).

[33] B. Keimer, N. Belk, R. J. Birgeneau, A. Cassanho, C. Y. Chen, M. Greven, M. A. Kastner, A. Aharony, Y. Endoh, R. W. Erwin, and G. Shirane. Magnetic excitations in pure, lightly doped, and weakly metallic La_2CuO_4. Phys. Rev. B ***46,*** 14034–14053 (1992).

[34] X. Feng, and N. M. Harrison, Magnetic coupling constants from a hybrid density functional with 35% Hartree-Fock exchange. Phys. Rev. B **70,** 2–5 (2004).

[35] S. Yamamoto, T. Fujiwara, & Y. Hatsugai, Electronic structure of charge and spin stripe order in $La_{2-x}Sr_xNiO_4$ (x = 1/3, 1/2). Phys. Rev. B **76,** 165114 (2007).

[36] V. I. Anisimov, J. Zaanen, & O. K. Andersen, Band theory and Mott insulators: Hubbard U instead of Stoner I. Phys. Rev. B **44,** 943–954 (1991).

[37] S. Pesant, and M. Côté, DFT+U study of magnetic order in doped La_2CuO_4 crystals. Phys. Rev. B **84,** 1–7 (2011).

[38] M. V. Zimmermann, A. Vigliante, T. Niemöller, N. Ichikawa, T. Frello, J. Madsen, P. Wochner, S. Uchida, N. H. Andersen, J. M. Tranquada, D. Gibbs and J. R. Schneider. Hard – X-ray diffraction study of charge stripe order in $La_{1.48}Nd_{0.4}Sr_{0.12}CuO_4$. Europhys. Lett. **41,** 629–634 (1998).

[39] J. Lloyd-Hughes, D. Prabhakaran, A. T. Boothroyd, and M. B. Johnston, Low-energy collective dynamics of charge stripes in the doped nickelate $La_{2-x}Sr_xNiO_{4+y}$ observed with optical conductivity measurements. Phys. Rev. B **77,** 2–5 (2008).

[40] C. C. Homes, J. M. Tranquada, Q. Li, A. R. Moodenbaugh, & D. J. Buttrey, Mid-infrared conductivity from mid-gap states associated with charge stripes. Phys. Rev. B **67,** 184516 (2003).

[41] J. M. Tranquada, D. J. Buttrey, V. Sachan, & J. E. Lorenzo, Simultaneous ordering of holes and spins in $La_2NiO_{4.125}$. Phys. Rev. Lett. **73,** 1003–1006 (1994).

[42] P. Wochner, J. M. Tranquada, D. J. Buttrey, & V. Sachan, Neutron-diffraction study of stripe order in La_2NiO_{4+d} with d = 2/15. Phys. Rev. B **57,** 1066–1078 (1998).

[43] J. Tranquada, D. Buttrey, & V. Sachan, Incommensurate stripe order in $La_{2-x}Sr_xNiO_4$ with x=0.225. Phys. Rev. B **54,** 318–323 (1996).

[44] Y. S. Lee, R. J. Birgeneau, M. A. Kastner, Y. Endoh, S. Wakimoto, K. Yamada, R. W. Erwin, S.-H. Lee, and G. Shirane. Neutron-scattering study of spin-density wave order in the superconducting state of excess-oxygen-doped La_2CuO_{4+y}. Phys. Rev. B 60, 3643 (1999).

[45] V. Sachan, D. J. Buttrey, J. M. Tranquada, J. E. Lorenzo, & G. Shirane, Charge and spin ordering in $La_{2-x}Sr_xNiO_4$ with x = 0.135 and 0.20. Phys. Rev. B **51,** 12742–12746 (1995).

[46] S.-H. Lee, & S.-W. Cheong, Melting of Quasi-Two-Dimensional Charge Stripes in $La_{5/3}Sr_{1/3}NiO_4$, Phys. Rev. Lett. **79,** 2514–2517 (1997).

[47] R. Zhong, B. L. Winn, G. Gu, D. Reznik, & J. M. Tranquada, Evidence for a Nematic Phase in $La_{1.75}Sr_{0.25}NiO_4$. Phys. Rev. Lett. **118,** 177601 (2017).

[48] S. Anissimova, *et al.* Direct observation of dynamic charge stripes in $La_{2-x}Sr_xNiO_4$. Nat. Commun.

5, 3467 (2014).

[49] C. Weber, K. Haule, & G. Kotliar, Strength of correlations in electron- and hole-doped cuprates. Nat. Phys. **6,** 574–578 (2010).

[50] S. Baroni, S. de Gironcoli, A. D. Corso, & P. Giannozzi, Phonons and related properties of extended systems from density-functional perturbation theory. Rev. Mod. Phys. **73,** 52 (2000).

[51] See Supplemental Material at URL for details on how the values of U-J were chosen.

FIGURE CAPTIONS

Figure 1. Calculated hole charge density iso-surface (yellow) showing the CDW of the conduction band minimum for the z = ½ (001) Ni-O plane of LSNO. Slight interplanar correlation can be seen in the adjacent layer (see text). La is gray, Sr is light blue, Ni is green, and O is red. For interpretation of the references to color in this figure legend, the reader is referred to the web version of this article. The iso-surface corresponds to an isovalue equivalent to one unit of charge per unit cell volume.

Figure 2. Calculated hole charge density iso-surface (yellow) showing the CDW in LSCO of first fully-unoccupied band which can be seen localized in Cu-O planes (densities from all eight impurity bands appear identical). La is gray, Sr is light blue, Cu is green, and O is red. For interpretation of the references to color in this figure legend, the reader is referred to the web version of this article. The iso-surface corresponds to an isovalue equivalent to one unit of charge per unit cell volume.

Figure 3. Calculated hole charge density iso-surface showing the CDW as a 2D slice in LSNO at z = ½ of (001) plane. Periodicity of red (dense) region is half the unit cell. Spin is indicated by arrows, where gray arrows are frustrated sites. SDW periodicity is the entire length in the x (right-left) direction. Density ranges from zero (blue) to 70% of the isovalue in Figure 1 (red), before it is sampled in 2D.

Figure 4. Calculated hole charge density iso-surface showing the CDW as a 2D slice in LSCO at z = ½ of (001) plane. Periodicity of red (dense) region is half the unit cell. Spin is indicated by arrows, where gray circles are frustrated sites. SDW periodicity is the entire length in the x (right-left) direction. Density ranges from zero (blue) to 70% of the isovalue in Figure 2 (red), before it is sampled in 2D.

Figure 5. Electronic structure for both spin channels and optical transitions in LSNO. (a) Band

structure, (b) PDOS for non-stripe-centered Ni, (c) PDOS for stripe-centered Ni, (d) PDOS for O p (e) and imaginary parts of frequency-dependent dielectric function. Fermi energy taken as zero is shown by red dashed line.

Figure 6. Electronic structure for both spin channels of LSCO. (a) Band structure, (b) PDOS for non-stripe-centered Cu, (c) PDOS for stripe-centered Cu, (d) and PDOS for O p. Fermi energy taken as zero is shown by red dashed line.

TABLES

Table 1. Components of static dielectric tensors. The pure electronic contributions are listed with and without local-field effects. For comparison, experimental results of Filippi, et al. [14] are also given.

	Local Field Effects	XX	YY	ZZ
IPA Electronic Contribution	none	7.09	7.09	5.91
IPA Electronic Contribution	in DFT	6.90	6.90	5.71
DFPT ionic contribution	N/A	42.39	42.39	17.87
Total		49.29	49.29	23.58
Experiment @ T = 5 K		100		

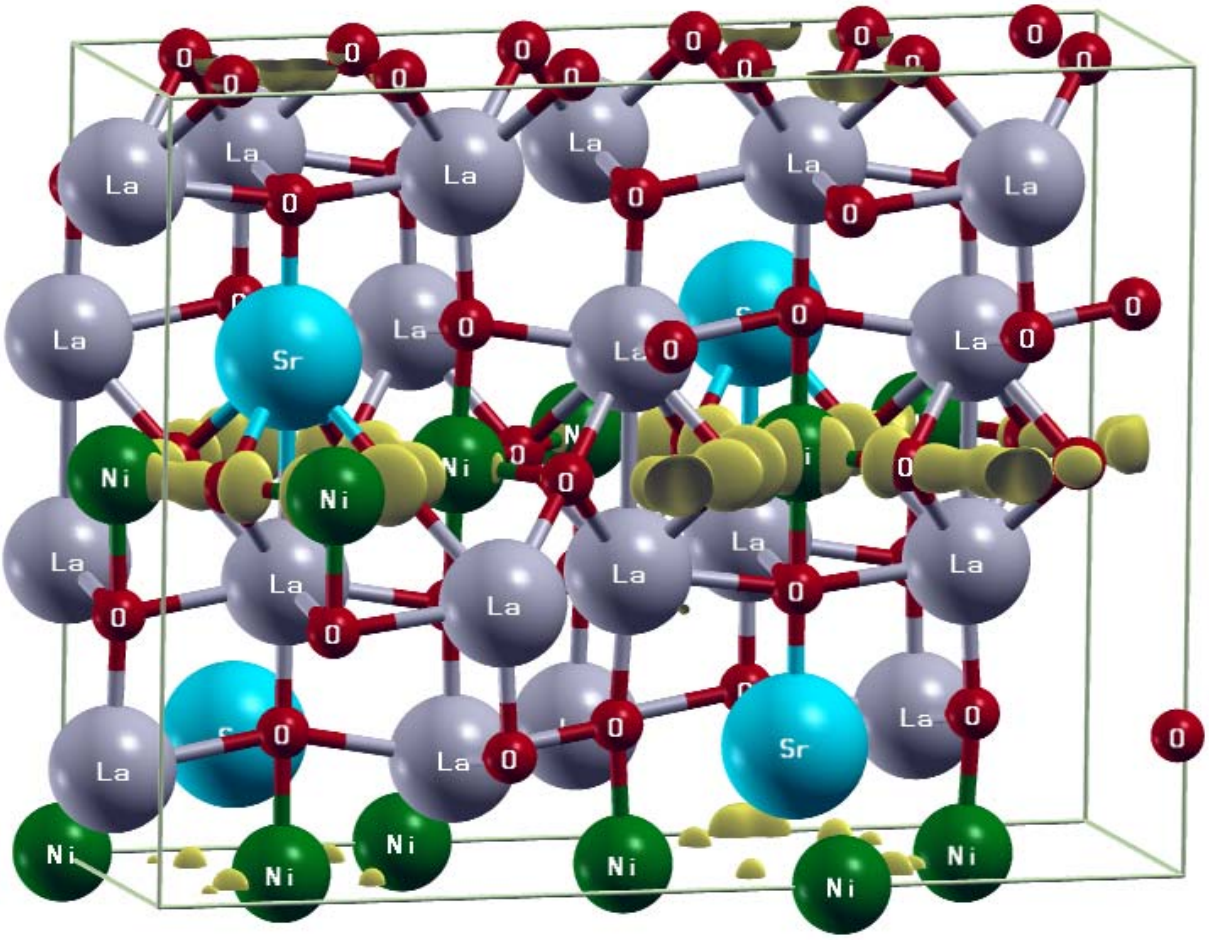

FIGURE 1

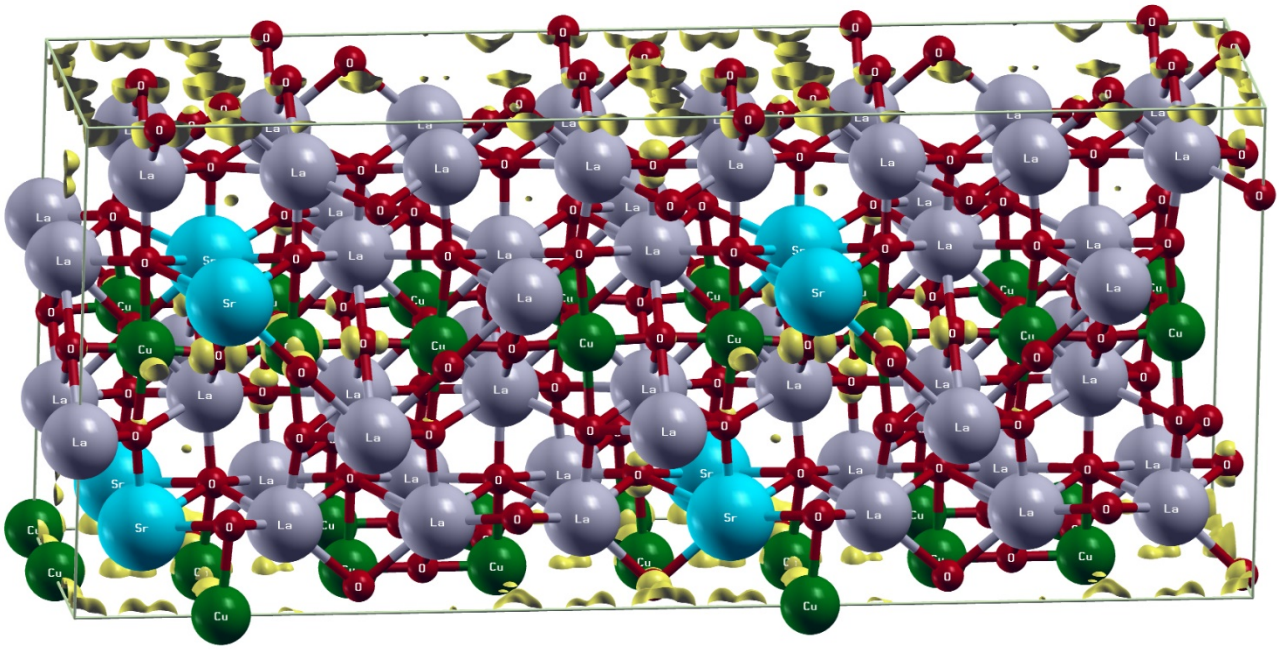

FIGURE 2

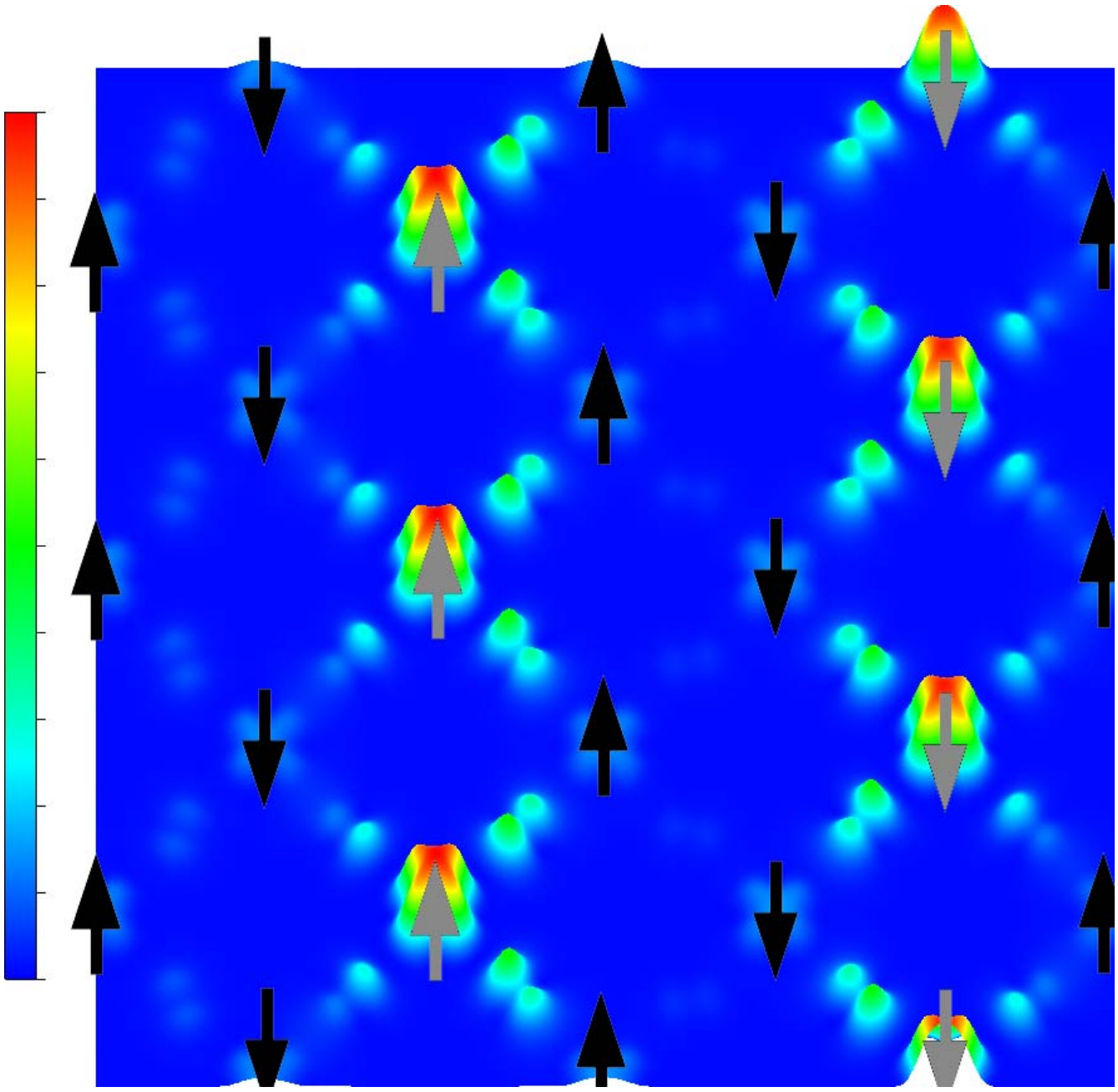

FIGURE 3

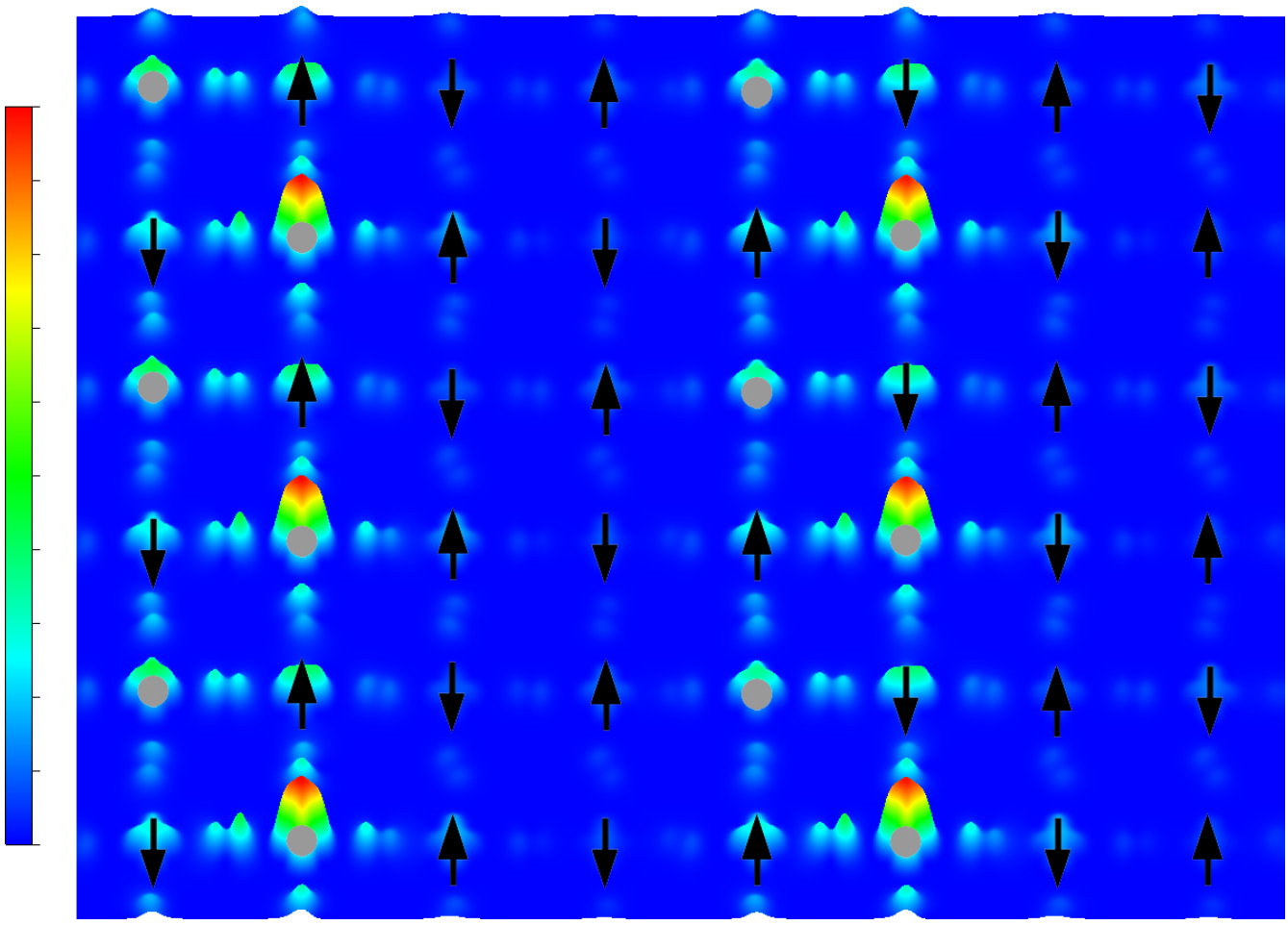

FIGURE 4

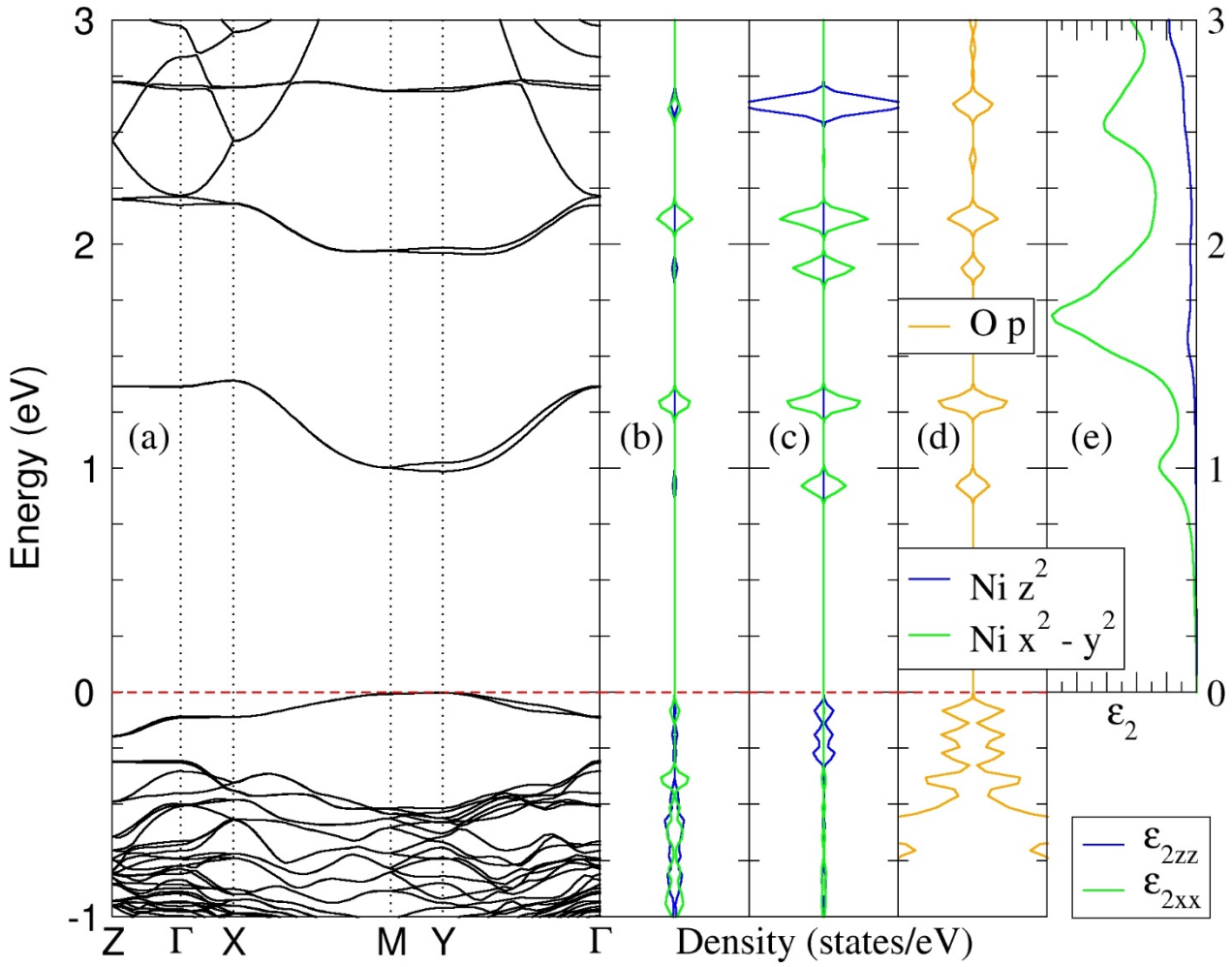
Energy (eV)
3
2
1
0
-1
Z
Γ
X
M
Y
Γ
(a)
(b)
(c)
(d)
(e)
O p
Ni z2
Ni x2 - y2
ε2
ε2zz
ε2xx
Density (states/eV)

FIGURE 5

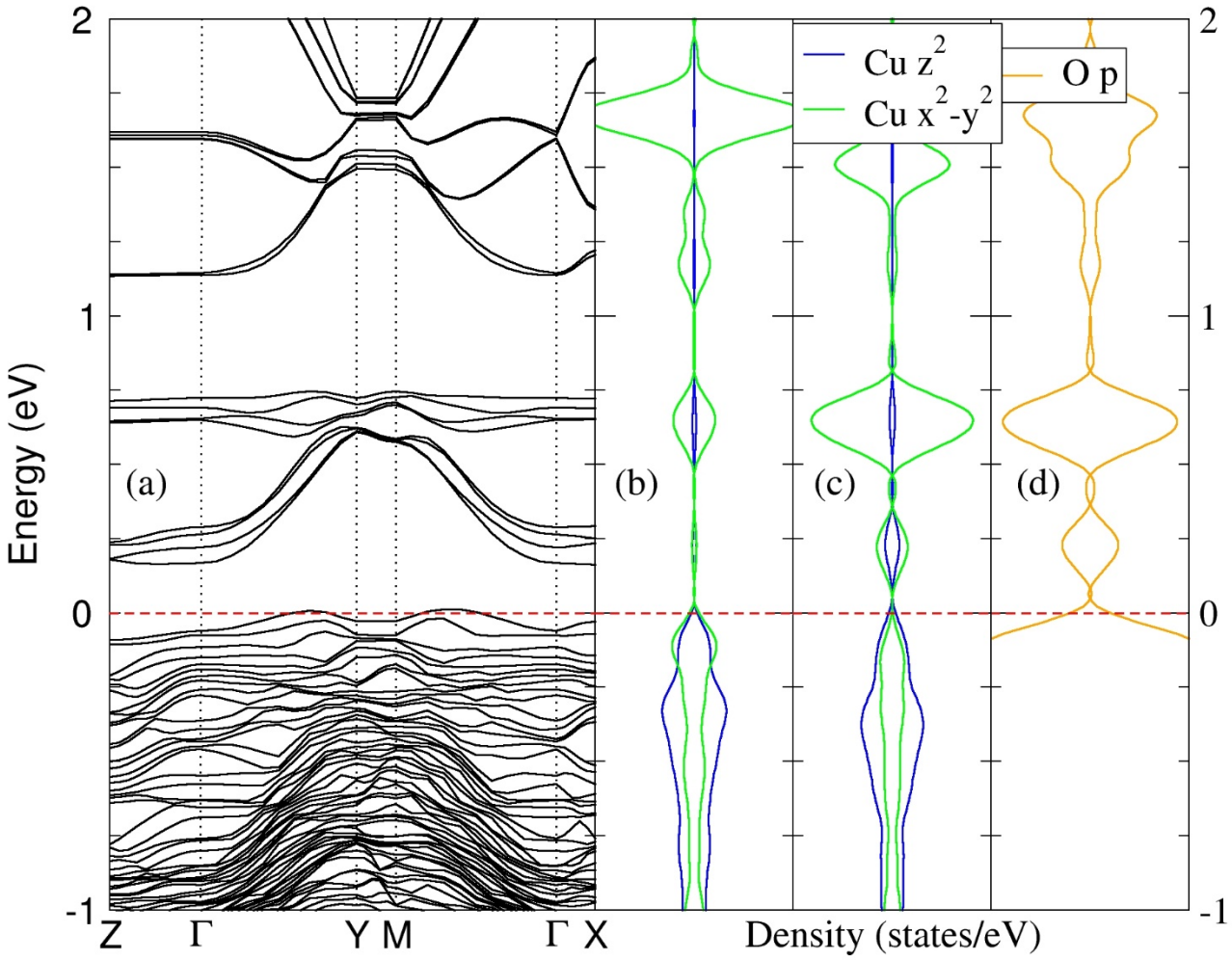

FIGURE 6